Article

Octanuclear Cubic Coordination Cages

Ian S. Tidmarsh, Thomas B. Faust, Harry Adams, Lindsay P. Harding, Luca Russo, William Clegg, and Michael D. Ward

J. Am. Chem. Soc., **2008**, 130 (45), 15167-15175 • DOI: 10.1021/ja805605y • Publication Date (Web): 15 October 2008

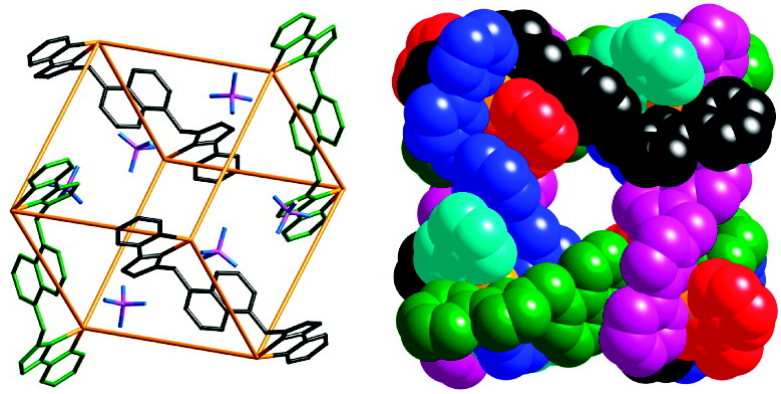

J|A|C|S
ARTICLES

Published on Web 10/15/2008

Octanuclear Cubic Coordination Cages

Ian S. Tidmarsh,[†] Thomas B. Faust,[†] Harry Adams,[†] Lindsay P. Harding,[‡] Luca Russo,[§] William Clegg,[§] and Michael D. Ward*[,†]

Department of Chemistry, University of Sheffield, Sheffield S3 7HF, U.K., Department of Chemical and Biological Sciences, University of Huddersfield, Huddersfield HD1 3DH, U.K., and School of Chemistry, Newcastle University, Newcastle upon Tyne NE1 7RU, U.K.

Received July 18, 2008; E-mail: m.d.ward@sheffield.ac.uk

Abstract: Two new bis-bidentate bridging ligands have been prepared, L^{naph} and L^{anth}, which contain two chelating pyrazolyl-pyridine units connected to an aromatic spacer (naphthalene-1,5-diyl and anthracene-9,10-diyl respectively) *via* methylene connectors. Each of these reacts with transition metal dications having a preference for octahedral coordination geometry to afford $\{M_8L_{12}\}^{16+}$ cages (for L^{anth}, M = Cu, Zn; for L^{naph}, M = Co, Ni, Cd) which have an approximately cubic arrangement of metal ions with a bridging ligand spanning each of the twelve edges, and a large central cavity containing a mixture of anions and/or solvent molecules. The cages based on L^{anth} have two cyclic helical $\{M_4L_4\}$ faces, of opposite chirality, connected by four additional L^{anth} ligands as "pillars"; all metal centers have a *meridional* tris-chelate configuration. In contrast the cages based on L^{naph} have (noncrystallographic) S_6 symmetry, with a diagonally opposite pair of corners having a *facial* tris-chelate configuration with the other six being *meridional*. An additional significant difference between the two types of structure is that the cubes containing L^{anth} do not show significant interligand aromatic stacking interactions. However, in the cages based on L^{naph}, there are six five-membered stacks of aromatic ligand fragments around the periphery, each based on an alternating array of electron-rich (naphthyl) and electron-deficient (pyrazolyl-pyridine, coordinated to M^{2+}) aromatic units. A consequence of this is that the cages $\{M_8(L^{naph})_{12}\}^{16+}$ retain their structural integrity in polar solvents, in contrast to the cages $\{M_8(L^{anth})_{12}\}^{16+}$ which dissociate in polar solvents. Consequently, the cages $\{M_8(L^{naph})_{12}\}^{16+}$ give NMR spectra in agreement with the symmetry observed in the solid state, and their fluorescence spectra (for M = Cd) display (in addition to the normal naphthalene-based $\pi-\pi^*$ fluorescence) a lower-energy exciplex-like emission feature associated with a naphthyl → pyrazolyl-pyridine charge-transfer excited state arising from the π-stacking between ligands around the cage periphery.

1. Introduction

The study of self-assembled coordination cages has become very popular in the last 15 years or so, partly because of their aesthetically appealing structures which illustrate the power of self-assembly as a synthetic tool and partly because of their host−guest chemistry which allows the cages to act as "micro-reactors" in some cases.[1−9] Several groups have shown how guest molecules in the cavities of the cages can behave, in terms of reactivity and stability, in ways that are quite different from the behavior shown by the same molecules when unconfined.[4] Thus, appealing form has developed into useful function.

In this paper we describe a new series of cages, with the structures of M_8L_{12} cubes that incorporate a different type of functionality: they are photophysically active by virtue of the fluorescent organic groups (naphthalene or anthracene) that are incorporated into the ligands' backbones. The ligands themselves are members of a series that we have studied extensively, containing two bidentate pyrazolyl-pyridine chelating units attached to an aromatic central group *via* flexible methylene

[†] University of Sheffield.
[‡] University of Huddersfield.
[§] Newcastle University.

(1) Reviews on coordination cages: (a) Swiegers, G. F.; Malefetse, T. J. *Coord. Chem. Rev.* **2002**, *225*, 91. (b) Fujita, M.; Tominaga, M.; Hori, A.; Therrien, B. *Acc. Chem. Res.* **2005**, *38*, 369. (c) Fiedler, D.; Leung, D. H.; Bergman, R. G.; Raymond, K. N. *Acc. Chem. Res.* **2005**, *38*, 349. (d) Hamilton, T. D.; MacGillivray, L. R. *Cryst. Growth Des.* **2004**, *4*, 419. (e) Ward, M. D. In *Organic Nanostructures*; Atwood, J., Steed, J., Eds.; Wiley: New York, 2008. (f) Garay, A. L.; Pichon, A.; James, S. L. *Chem. Soc. Rev.* **2007**, *36*, 846. (g) Alvarez, S. *Dalton Trans.* **2006**, 2209. (h) Saalfrank, R. W.; Uller, E.; Demleitner, B.; Bernt, I. *Struct. Bonding (Berlin)* **2000**, *96*, 149. (i) Stang, P. J.; Seidel, S. R. *Acc. Chem. Res.* **2002**, *35*, 972. (j) Saalfrank, R. W.; Demleitner, B. In *Perspectives in Supramolecular Chemistry*; Sauvage, J.-P., Ed.; John Wiley & Sons Ltd.: Chichester, U.K., 1999; Vol. 5, pp 1−51.

(2) (a) Sun, X. K.; Johnson, D. W.; Caulder, D. L.; Raymond, K. N.; Wong, E. H. *J. Am. Chem. Soc.* **2001**, *123*, 2752. (b) Fujita, M.; Umemoto, K.; Yoshizawa, M.; Fujita, N.; Kusukawa, T.; Biradha, K. *Chem. Commun.* **2001**, 509. (c) Caulder, D. A.; Raymond, K. N. *J. Chem. Soc., Dalton Trans.* **1999**, 1185.

(3) (a) Davis, A. V.; Fiedler, D.; Seeber, G.; Zahl, A.; van Eldik, R.; Raymond, K. N. *J. Am. Chem. Soc.* **2006**, *128*, 1324. (b) Johnson, D. W.; Raymond, K. N. *Inorg. Chem.* **2001**, *40*, 5157. (c) Paul, R. L.; Bell, Z. R.; Jeffery, J. C.; McCleverty, J. A.; Ward, M. D. *Proc. Natl. Acad. Sci. U.S.A.* **2002**, *99*, 4883. (d) Brassey, T.; Scopelliti, R.; Severin, K. *Chem. Commun.* **2006**, 3308. (e) Hiraoka, S.; Kubota, Y.; Fujita, M. *Chem. Commun.* **2000**, *16*, 1509.

(4) (a) Yamaguchi, T.; Fujita, M. *Angew. Chem., Int. Ed.* **2008**, *47*, 2067. (b) Nishioka, Y.; Yamaguchi, T.; Yoshizawa, M.; Fujita, M. *J. Am. Chem. Soc.* **2007**, *129*, 7000. (c) Takaoka, K.; Kawano, M.; Ozeki, T.; Fujita, M. *Chem. Commun.* **2006**, 1625. (d) Yoshizawa, M.; Fujita, M. *Pure Appl. Chem.* **2005**, *77*, 1107. (e) Koblenz, T. S.; Wassenaar, J.; Reek, J. N. H. *Chem. Soc. Rev.* **2008**, *37*, 247. (f) Kleij, A. W.; Reek, J. N. H. *Chem. Eur. J.* **2006**, *12*, 4219. (g) Leung, D. H.; Bergman, R. G.; Raymond, K. N. *J. Am. Chem. Soc.* **2006**, *128*, 9781.

Chart 1

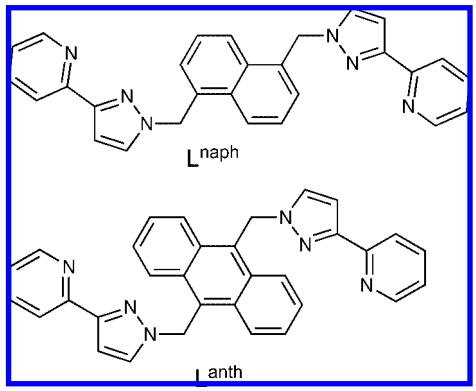

hinges (Chart 1).[1e] A recurrent feature of the coordination chemistry of these ligands is their tendency, when combined with labile metal cations which have a preference for octahedral coordination geometry, to form elaborate cages with a 2M:3L ratio. This ratio is a simple consequence of the fact that each ligand provides four donor atoms, whereas each metal ion requires six, such that 1.5 ligands per metal ion are required for a coordinatively saturated assembly. These M:L proportions also neatly reflect the fact that many polyhedral shapes have a 2:3 ratio of vertices to edges, such that the stoichiometric requirements of the cages can be met by adoption of a polyhedral shape in which each metal ion occupies one vertex of the polyhedron and each bridging ligand spans one edge. Thus, we have isolated examples of M_4L_6 tetrahedra,[3c,5b,c] M_8L_{12} cubes,[7] $M_{12}L_{18}$ truncated tetrahedra,[8] and $M_{16}L_{24}$ tetra-capped truncated tetrahedra,[9a] all based on bis-bidentate bridging ligands and all with a 2M:3L proportion having a metal ion at each vertex and a bridging ligand along each edge.

A very common structural feature of all of these cages that we have prepared so far is aromatic stacking, usually with the central aromatic spacer from the ligand alternating with coordinated pyrazolyl-pyridine units: i.e. stacks of relatively electron-poor and electron-rich aromatic fragments alternating with one another. In a recent communication we showed how, if the central aromatic spacer of the ligand is a fluorescent naphthyl unit, this stacking results in a red-shifted excimer-like luminescence which does not exist for the free ligand but which is characteristic of the assembled cage.[10] Accordingly, we were interested in further examination of the properties of cages incorporating aromatic fluorophores into the ligand superstructure. In addition to the possibility of modified fluorescence due to π-stacking being used as a reporter of cage assembly, there is the possibility of preparing cages with large central cavities surrounded by an array of fluorophores which could (for example) act as excited state energy- or electron-donors to trapped guest molecules in the central cavity. We describe here the syntheses, structures, solution properties, and photophysical behavior of two series of complexes, one containing naphthyl and the other containing anthracenyl fluorophores.

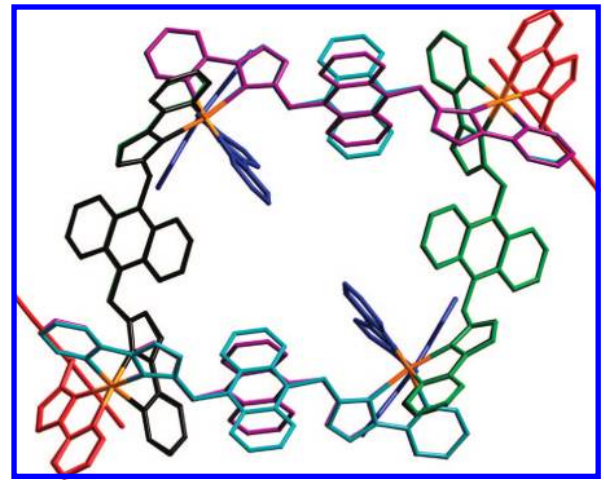

Figure 1. Structure of the complex cation of $[Zn_8(L^{anth})_{12}][BF_4]_{16}\cdot 15MeNO_2\cdot Et_2O$ with ligands colored differently for clarity. Zn(II) centers are in orange; the pairs of symmetry-equivalent ligands have the same color.

2. Results and Discussion

2.1. Ligand Syntheses. The ligand syntheses (see Chart 1 for structural formulas) used our standard method:[1e] reactions of 2 equiv of 3-(2-pyridyl)pyrazole with 9,10-bis(bromomethyl)anthracene for L^{anth}, and with 1,5-bis(bromomethyl)naphthalene for L^{naph}, under basic conditions to deprotonate the pyrazole. In addition to characterization by standard spectroscopic and analytical methods (see Experimental Section), both ligands were structurally characterized by X-ray crystallography (see Supporting Information).

2.2. Structures of Complexes with L^{anth}. Reaction of L^{anth} with $Cu(BF_4)_2$ or $Zn(BF_4)_2$, either by conventional solution methods or by solvothermal methods, resulted in each case in a crop of small X-ray quality crystals whose elemental analysis was (as expected) approximately consistent with the empirical formulation $M_2(L^{anth})_3(BF_4)_4$. The crystal structures revealed the complexes to be octanuclear cages.

The structure of $[Zn_8(L^{anth})_{12}](BF_4)_{16}$ is shown in Figures 1 and 2. The eight metal ions form an approximately cubical array, with Zn···Zn separations along the edges lying in the range 12.27−13.55 Å. The cage lies astride a center of symmetry such that half of it (four metal cations and six ligands) is crystallographically unique. The "cube" is slightly slanted (Figure 1) with Zn−Zn−Zn angles in the slanted faces lying in the range

(5) (a) Saalfrank, R. W.; Burak, R.; Breit, A.; Stalke, D.; Herbst-Irmer, R.; Daub, J.; Porsch, M.; Bill, E.; Muther, M.; Trautwein, A. X. *Angew. Chem., Int. Ed. Engl.* **1994**, *33*, 1621. (b) Fleming, J. S.; Mann, K. L. V.; Carraz, C.-A.; Psillakis, E.; Jeffery, J. C.; McCleverty, J. A.; Ward, M. D. *Angew. Chem., Int. Ed.* **1998**, *37*, 1279. (c) Paul, R. L.; Argent, S. P.; Jeffery, J. C.; Harding, L. P.; Lynam, J. M.; Ward, M. D. *Dalton Trans.,* **2004**, 3453. (d) Clegg, J. K.; Lindoy, L. F.; Moubaraki, B.; Murray, K. S.; McMurtrie, J. C. *Dalton Trans.,* **2004**, 2417. (e) Davis, A. V.; Fiedler, D.; Ziegler, M.; Terpin, A.; Raymond, K. N. *J. Am. Chem. Soc.,* **2007**, *129*, 15354.

(6) (a) Amoroso, A. J.; Jeffery, J. C.; Jones, P. L.; McCleverty, J. A.; Thornton, P.; Ward, M. D. *Angew. Chem., Int. Ed. Engl.* **1995**, *34*, 1443. (b) Albrecht, M.; Janser, I.; Burk, S.; Weis, P. *Dalton Trans.* **2006**, 2875. (c) Yeh, R. M.; Xu, J.; Seeber, G.; Raymond, K. N. *Inorg. Chem.* **2005**, *44*, 6228.

(7) (a) Bell, Z. R.; Harding, L. P.; Ward, M. D. *Chem. Commun.* **2003**, 2432. (b) Argent, S. P.; Adams, H.; Harding, L. P.; Ward, M. D. *Dalton Trans.* **2006**, 542.

(8) (a) Bell, Z. R.; Jeffery, J. C.; McCleverty, J. A.; Ward, M. D. *Angew. Chem., Int. Ed.* **2002**, *41*, 2515. (b) Argent, S. P.; Adams, H.; Riis-Johannessen, T.; Jeffery, J. C.; Harding, L. P.; Mamula, O.; Ward, M. D. *Inorg. Chem.* **2006**, *45*, 3905.

(9) (a) Argent, S. P.; Adams, H.; Riis-Johannessen, T.; Jeffery, J. C.; Harding, L. P.; Ward, M. D. *J. Am. Chem. Soc.* **2006**, *128*, 72. (b) Al-Rasbi, N. K.; Tidmarsh, I.; Argent, S. P.; Adams, H.; Harding, L. P.; Ward, M. D. *J. Am. Chem. Soc.* **2008**, *130*, 11641.

(10) Al-Rasbi, N. K.; Sabatini, C.; Barigelletti, F.; Ward, M. D. *Dalton Trans.* **2006**, 4769.

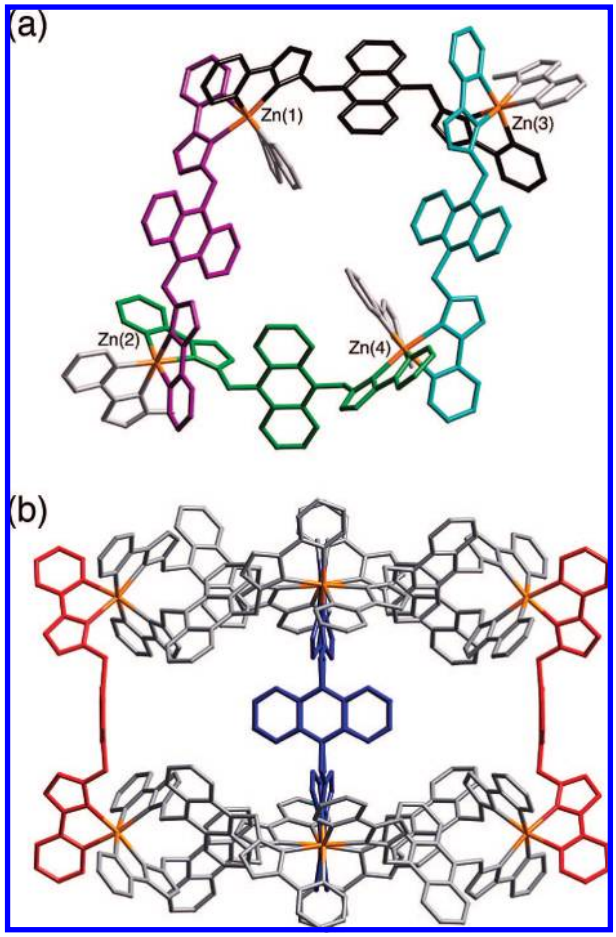

Figure 2. (a) Partial view of the complex cation of $[Zn_8(L^{anth})_{12}][BF_4]_{16}\cdot 15MeNO_2\cdot Et_2O$ showing one tetranuclear cyclic helical face. The ligand fragments shown in gray are the "pillars" which connect the top and bottom cyclic helical faces [these ligands are shown in blue and red in (b)]. (b) View orthogonal to that shown in (a) in which the two tetranuclear cyclic helicates are now shown in gray at the top and bottom of the picture, with the four "pillars" (two equivalent pairs) shown in red and blue. The second blue ligand, at the back of this view, is eclipsed by the first one.

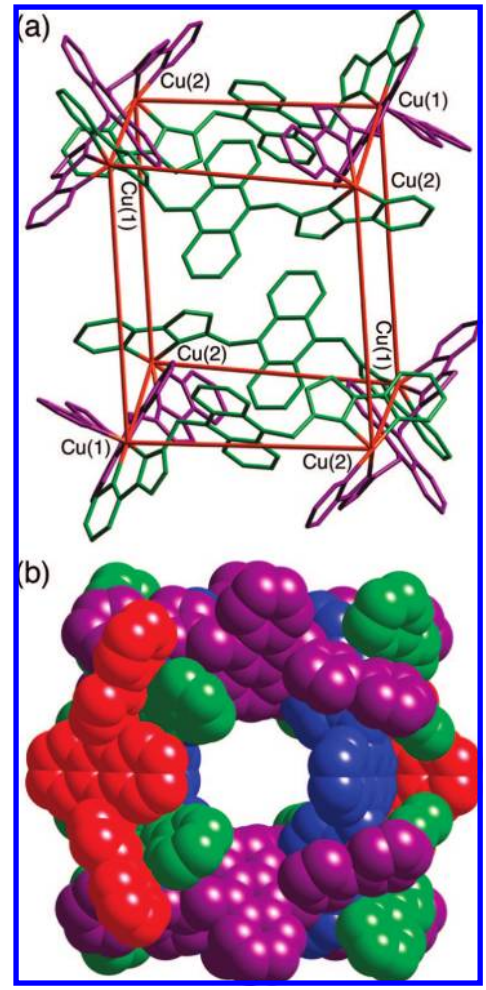

Figure 3. (a) Partial view of the complex cation of $[Cu_8(L^{anth})_{12}][BF_4]_{16}\cdot 10MeNO_2$ emphasizing the approximately cubic array of metal ions. The two tetranuclear cyclic helical fragments have their ligands included; crystallographically equivalent ligands have the same color. The four vertical "pillars" connecting these two faces are not shown for clarity. (b) Space-filling view of the complete cubic cage.

67.5−112.3°. The twelve ligands lie along the Zn···Zn edges, each ligand spanning two metal ions. There is no significant aromatic stacking involving any of the ligand fragments, which is unusual in our experience. Two anions could be located inside the cavity, although due to extensive disorder of anions and solvent molecules (only 10 of the expected 16 $[BF_4]^-$ anions could be located, for example) it is not possible to be definitive about what else is in the cavity.

All four crystallographically independent metal centers have a *meridional* tris-chelate coordination geometry. The Zn−N distances are unremarkable, lying in the range 2.10−2.26 Å. All four independent metal centers Zn(1)−Zn(4) have the same absolute configuration associated with the tris-chelate coordination geometry, such that the face containing Zn(1), Zn(2), Zn(3), and Zn(4) constitutes a cyclic helical array with the four bridging ligands around that face having the same "under and over" twisted arrangement necessary to propagate the helical structure [Figure 2a]. On the opposite face [Zn(1A)−Zn(4A), generated by inversion] the four metal ions are all the opposite enantiomers. The two cyclic helical faces are then joined by four perpendicular "column" ligands (red and blue in Figure 2) which are not twisted and link the two helical layers. Overall, therefore, the cage is achiral. It is also quite different in its symmetry from the previous examples we described that have approximate S_6 symmetry.[7] Significantly, in this case (unlike all of the other cages of this family that we have structurally characterized) there is no significant π-stacking between ligands to stabilize the cage structure. The central cavity is an irregular shape with distances between symmetry-equivalent pairs of H atoms on either side of the central cavity varying between 10 and 22 Å, depending on which pair of ligands is chosen; taking a somewhat arbitrary average diameter of 15 Å and allowing for the size of the H atoms, this gives a cavity size of the order of 1000 $Å^3$.

The analogous Cu(II) complex has essentially the same structure, although it crystallizes in a higher-symmetry space group (*C2/m)* such that the cage has C_{2h} rather than inversion symmetry, with one-quarter of the complex (two metal ions and three ligands) being crystallographically independent (Figure 3). Apart from that, the above discussion regarding the structure and symmetry of the Zn(II) complex applies to the Cu(II) cage. The coordination geometry around the Cu(II) ions is more irregular than it was around the Zn(II) ions, with Cu−N distances in the range 2.00−2.42 Å and each of the two independent Cu(II) ions showing the usual Jahn−Teller distorted geometry with four short bonds in a plane (average distance 2.02 Å) and an axially elongated pair (average distance 2.35

Å). Clearly this irregularity in the coordination geometry around the Cu(II) ions is not sufficient to prevent the cage from forming. Again, extensive disorder of solvent molecules and counterions prevented all of these from being located, but the structure of the cationic complex cage is clear.

Attempts to characterize these complexes in solution by electrospray mass spectrometry (ESMS) and ^{1}H NMR spectroscopy were unsuccessful. No peaks for the intact cages could be observed by ESMS, even under mild conditions, with by far the most intense peak in each case corresponding to the species $\{M(L^{anth})_2F\}^+$ (fluoride presumably arising from the terafluoroborate counterions). In agreement with this, the ^{1}H NMR spectrum of $[Zn_8(L^{anth})_{12}](BF_4)_{16}$ was broad and poorly resolved, indicating a mixture of slowly interconverting species in solution, presumably arising from fragmentation of the cage. This may be associated with the lack of stabilizing π-stacking interactions involving the ligands (see below) and means that, although the solid-state structures of these cages are interesting, there is no possibility of studying their host−guest or spectroscopic properties in solution.

2.3. Structures of Complexes with L^{naph}. Reaction of L^{naph} with $Co(BF_4)_2$ or $Ni(BF_4)_2$ in MeOH under solvothermal conditions followed by slow cooling afforded a crop of X-ray quality crystals in each case, whose elemental analysis indicated the expected empirical formula $[M_2(L^{naph})_3][BF_4]_4$. On X-ray crystallographic analysis these also proved to be M_8L_{12} cubic cages, but with some significant structural differences compared to the previous series. We also prepared the analogous complex with Cd(II) and characterized it by NMR spectroscopy and mass spectrometry, although this complex did not give X-ray quality crystals and so was not structurally characterized.

The crystal structure of $[Co_8(L^{naph})_{12}][BF_4]_{16}$ is shown in Figures 4 and 5. The complex crystallizes in space group *C*2/*c* such that the cage lies on an inversion center, with four metal ions and six ligands being crystallographically independent. As before, the metal ions form an approximately cubical array with a bridging ligand along each edge. The metal cube is more regular than before, with Co···Co separations along the edges lying in the range 10.86−11.58 Å, and all Co−Co−Co angles at corners lying between 85 and 95°. Figure 4 shows the cubic framework with only four of the bridging ligands (two crystallographically equivalent pairs, related by inversion) shown for clarity. Figure 4 also includes six of the tetrafluoroborate anions, which are located in the center of each face, effectively blocking the "windows" into the center of the cavity. The central cavity contains four methanol molecules (not shown).

There are several features of this structure which are noteworthy. First, in notable contrast to the cages based on L^{anth}, all of the ligands are involved in extensive π-stacking around the periphery of the cage. This is emphasized in Figure 5, with arrows showing two of the sets of five-component stacks. Each stack is based on an alternating sequence of three pyridyl-pyrazole [electron-deficient, being coordinated to Co(II) ions] and two naphthyl (electron-rich) components. There are six such stacks, such that all twelve naphthyl groups from the L^{naph} ligands are each sandwiched between two pyridyl-pyrazole units. In addition to the two sets of stacks marked by the arrows in Figure 5, there are two more running into the page (in the sequence cyan−black−red−blue−cyan, at the top and bottom of the figure) and two running from bottom left to top right (purple−green−blue−cyan−purple, edge-on in the figure).

This stacking of alternately electron-rich and electron-deficient aromatic components is a feature of these cage complexes that commonly recurs[7−10] and is well-known to result in particularly strong aromatic stacking interactions in which a charge-transfer

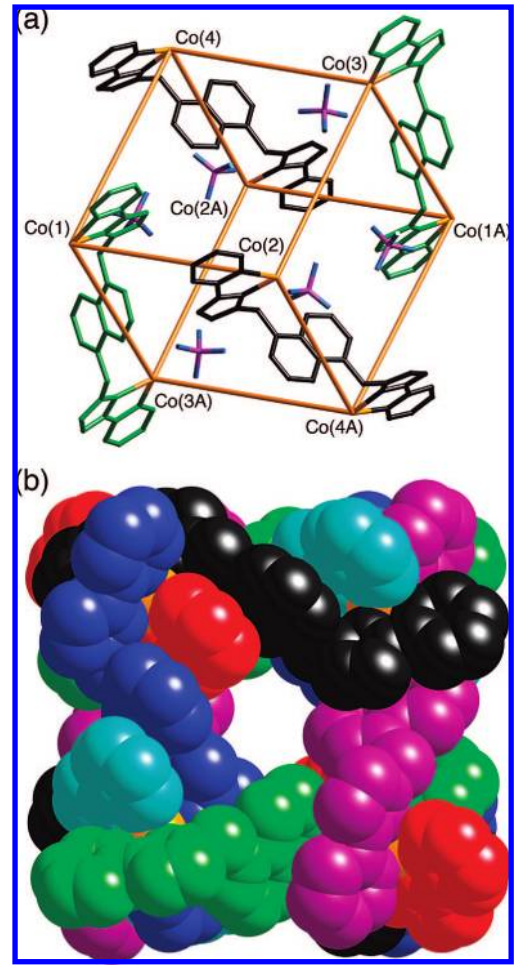

Figure 4. (a) Partial view of the complex cation of $[Co_8(L^{naph})_{12}][BF_4]_{16}\cdot 6MeOH$, emphasizing the approximately cubic array of metal ions. Only four of the twelve ligands (two equivalent pairs) are shown. The tetrafluoroborate anions shown are those that occupy the spaces in the center of each of the six faces of the cube. (b) Space-filling view of the complete cubic cage.

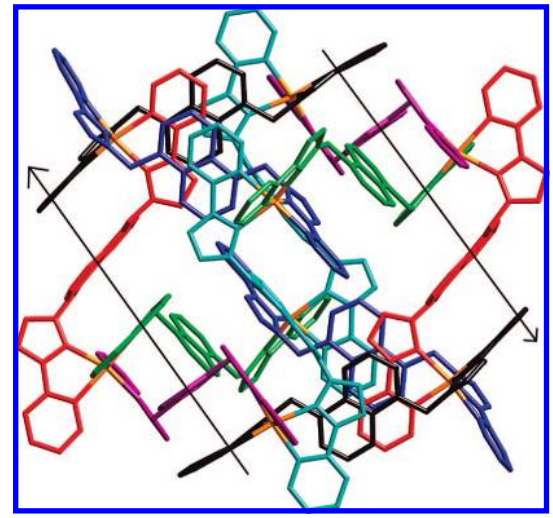

Figure 5. An alternative view of the complex cation of $[Co_8(L^{naph})_{12}][BF_4]_{16}\cdot 6MeOH$ emphasizing the alternating aromatic stacking of napthyl/pyridyl-pyrazole units. Two of the six stacks are highlighted by arrows. Crystallographically equivalent ligands have the same color.

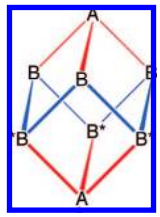

Figure 6. Sketch of the cubic framework of the cage cations in $[M_8(L^{naph})_{12}][BF_4]_{16}$ emphasizing the (noncrystallographic) S_6 symmetry. Labels **A** and **B** denote the *facial* and *meridional* tris-chelate metal centers, respectively; * denotes an opposite enantiomer, such that **A** and **A*** are enantiomers of one another. The two types of edge environment (i.e., bridging ligands) are colored separately.

component is significant.[11,12] Indeed such heterostacking has been used extensively by Stoddart and co-workers to preorganize electron-rich (naphthalenes) and electron-poor (viologens) aromatic components in formation of catenanes and other topologically novel species.[12] The sandwiching of one 2+ charged viologen unit between two electron-rich aromatic rings, to give a D−A−D (D = donor, A = acceptor) three-layer stack with two favorable D−A interactions, was measured to have a free energy change of around −16 kJ mol^{-1}. In the structures of $[Co_8(L^{naph})_{12}][BF_4]_{16}$ there are 24 such interactions, from four pairwise D−A interactions in each of six sets of stacks around the periphery of the complex. Even though the partial positive charge on each chelating pyridyl-pyrazole unit in the cube complex is less than the 2+ charge of a viologen in Stoddart's systems, because the 2+ charge of each metal ion is shared between the metal center itself and three coordinated pyridyl-pyazole units, this alternating D/A stacking motif must provide a substantial driving force for cage assembly.

A second feature of interest in the structure is the choice of geometric isomers at the metal centers. Although all metal ions have typical pseudo-octahedral tris-chelate coordination geometries, with Co−N distances in the range 2.11−2.20 Å [characteristic of high-spin Co(II)], their configurations are different. Co(1), Co(3), and Co(4) have meridional tris-chelate geometries, whereas Co(2) is facial. In addition, Co(1), Co(3), and Co(4) all have the same absolute configuration, whereas Co(2) has the opposite one. This leads to the situation sketched in Figure 6 from which it will be apparent that the cage has (noncrystallographic) S_6 symmetry with the principal rotation axis being the Co(2)···Co(2A) vector. This is clearly different from the behavior shown by the $[M_8(L^{anth})_{12}](BF_4)_{16}$ cages, but is similar to what we observed with the M_8L_{12} cages we described earlier with different ligands.[7]

The structure of $[Ni_8(L^{naph})_{12}][BF_4]_{16}$ is essentially identical, being crystallographically isostructrural and isomorphous, and all of the comments above apply equally to both Co(II) and Ni(II) versions of the cubic cage. The Ni−N distances lie in the range 2.09−2.17 Å.

2.4. Solution Characterization of Complexes with L^{naph}. Electrospray mass spectrometric studies on $[M_8(L^{naph})_{12}][BF_4]_{16}$ (M = Co, Ni, Cd) confirmed that the complexes remain assembled in solution, with a clear sequence of peaks being observed for the species $\{M_8(L^{naph})_{12}][BF_4]_{16-n}\}^{n+}$ with n typically in the range 3−10, as the intact cage cation remains associated with varying numbers of tetrafluoroborate anions. A sample spectrum [of the Co(II) cage] in Figure 7 clearly shows

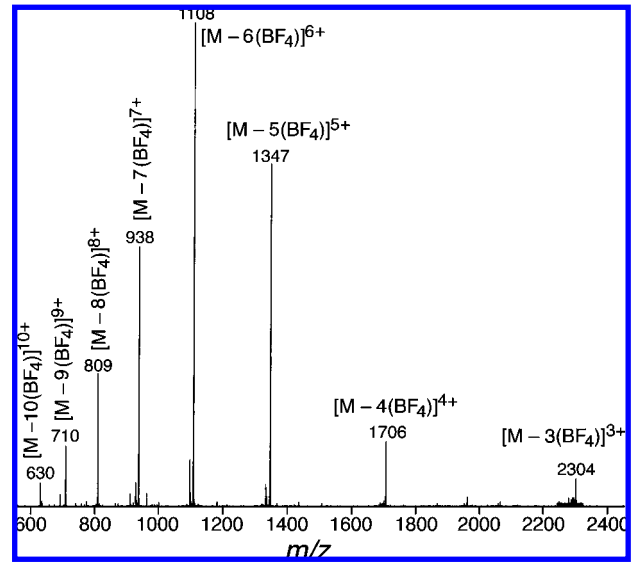

Figure 7. Electrospray mass spectrum of $[Co_8(L^{naph})_{12}][BF_4]_{16}$ showing a sequence of peaks corresponding to loss of 3−10 anions from the complete complex (**M**).

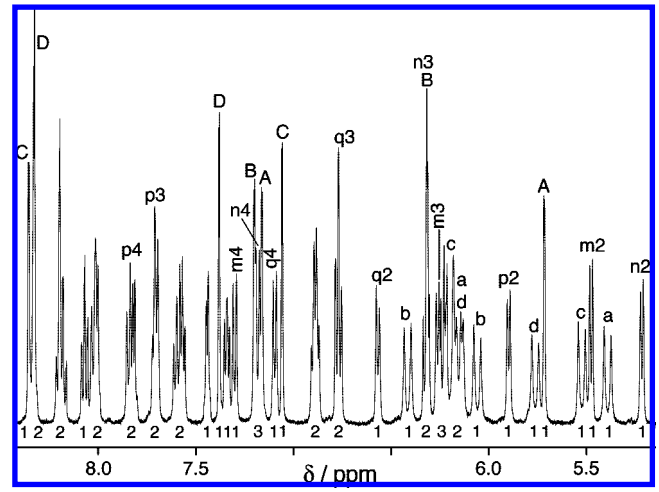

Figure 8. 500 MHz ^{1}H NMR spectrum of $[Cd_8(L^{naph})_{12}][BF_4]_{16}$ in CD_3NO_2 showing the 44 inequivalent signals required by the crystal structure. Partial assignments (diastereotopic pairs of CH_2 protons, a/b/c/d; pyrazolyl protons, A/B/C/D; naphthyl protons, *n*2/*n*2/*n*4, etc., see main text) were based on a COSY spectrum.

the entire sequence of peaks arising from loss of 3−10 anions from the complete assembly.

In order to examine the solution properties of these cages more thoroughly by NMR methods, we examined the diamagnetic analogue $[Cd_8(L^{naph})_{12}][BF_4]_{16}$ by both ^{1}H and ^{113}Cd NMR spectroscopy. The ^{1}H NMR spectrum of $[Cd_8(L^{naph})_{12}][BF_4]_{16}$ is shown in Figure 8 and is clearly consistent with the cubic cage structure being retained in solution. Based on Figure 6 there should be two ligand environments: six ligands spanning metal types A−B or A*−B* and six more ligands spanning metal types B−B*. Clearly along the A−B edges both ends of each ligand will be different, leading to 22 inequivalent proton environments (each corresponding to 6H). The symmetry of six ligands spanning the B−B* edges is less obvious. It might be expected (based on Figure 6) that each of these ligands should have two-fold internal symmetry with the ends equivalent, giving 11 resonances each of double intensity (i.e., each corresponding to 12H). However, each ligand adopts a helical twist on

(11) Hunter, C. A.; Sanders, J. K. M. *J. Am. Chem. Soc.* **1990**, *112*, 5525.
(12) Claessens, C. G.; Stoddart, J. F. *J. Phys. Org. Chem.* **1997**, *10*, 254.

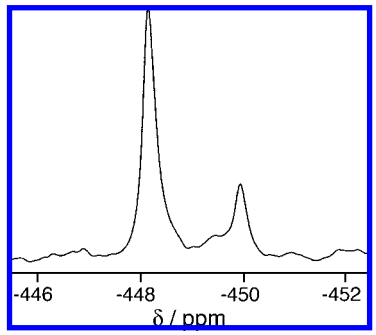

Figure 9. ^{113}Cd NMR spectrum of $[Cd_8(L^{naph})_{12}][BF_4]_{16}$ in CD_3NO_2 showing the presence of two Cd environments in an approximately 1:3 ratio (cf. Figure 6).

coordination, which results in symmetry breaking. Since the two ends of the ligand, each having the same sense of helical twist, coordinate to metal ions of opposite chirality (B and B*), it follows that the two ligand ends will be inequivalent (cf. the inequivalence of diastereosiomers). Thus, this set of six ligands also generates 22 independent proton environments. The total will be 44 inequivalent proton signals, which is what is seen in the ^{1}H NMR spectrum. Although not all of the signals can be assigned due to substantial overlapping of signals (even at 500 MHz), from the COSY spectrum we can readily assign four coupled pairs of pyrazole H^3/H^4 protons from the four inequivalent pyrazolyl rings (labeled on Figure 8 as A, B, C, D; these doublets are characterized by very small coupling constants). The four pairs of diastereotopic CH_2 protons can also be readily assigned from the COSY spectrum (labeled as a, b, c, d; these have much larger coupling constants). We can also assign four sets of three coupled protons (doublet, triplet, doublet) corresponding to the four independent $H^2/H^3/H^4$ sets of protons from the naphthyl rings: these are labeled as *m*2/*m*3/*m*4, *n*2/*n*3/*n*4 etc. in Figure 7. The occurrence of some of these naphthyl-based resonances at chemical shifts as low as 5.2 ppm is consistent with the aromatic stacking between naphthyl groups and adjacent pyrazolyl-pyridine groups. The remaining protons forming the pyridyl rings are not individually assigned, but it is clear from this spectrum that the cage structure of $[Cd_8(L^{naph})_{12}][BF_4]_{16}$ is retained in solution with S_6 symmetry as was apparent from the crystal structures of the Co(II) and Ni(II) complexes. A consequence of the S_6 symmetry (Figure 6) is that there are two metal ions of type A (*facial* tris-chelate coordination geometry) and six of type B (*meridional* tris-chelate coordination geometry). The ^{113}Cd NMR spectrum should therefore show two Cd environments in a 3:1 ratio, and this is indeed the case (Figure 9).

Finally in this section, we also recorded the ^{1}H NMR spectrum of the paramagnetic cage $[Co_8(L^{naph})_{12}][BF_4]_{16}$, which was structurally characterized (see above). High-spin Co(II) complexes give highly shifted ^{1}H NMR spectra, but with the peaks remaining sharp enough to be individually identified, so they have substantial diagnostic value.[3c,13] The intensity and degree of broadening of individual peaks varies, depending on the distance from the paramagnetic centers of the protons concerned, but it is clear that 44 signals can be identified at chemical shifts between +118 and −90 ppm (Figure 10), confirming that this complex also retains in solution the S_6 symmetry that was apparent in the solid state.

2.5. Luminescence Spectroscopy of $[Cd_8(L^{naph})_{12}][BF_4]_{16}$. The extensive aromatic stacking of the naphthyl groups in this cage is, on the basis of recent preliminary studies, expected to have a significant effect on their fluorescence, with the assembled cage showing different fluorescence properties from the free ligand in the form of a low-energy "exciplex-like" emission feature that does not occur for the free ligand.[10] Note that we only performed fluorescence studies on the Cd(II) complex because Co(II) and Ni(II) have low-energy electronic transitions which are expected to quench the naphthalene-based emission. We note that Shionoya and co-workers have recently described some fluorescent coordination cages.[14]

The UV/vis absorption and fluorescence spectra of the free ligand L^{naph} are shown in Figures 11 and 12a respectively. The main fluorescence band centered at 340 nm is unremarkable, being typical of substituted naphthalenes; it tails off completely by about 450 nm. The fluorescence spectrum of $[Cd_8(L^{naph})_{12}][BF_4]_{16}$ [Figure 12b] reveals significantly different behavior. In addition to the normal naphthalene-based fluorescence with a maximum at 340 nm, there is an additional lower-energy emission band, apparent as a shoulder at ~400 nm, which extends out beyond ~550 nm. This low-energy emission feature is absent in the fluorescence spectrum of L^{naph} and may be ascribed to exciplex-like emission from an excited state which has been stabilized by the aromatic stacking. We emphasize that this is not normal excimer or exciplex emission as these terms usually apply to diffusion-controlled processes between like partners (excimer formation) or different partners (exciplex formation).[15] In $[Cd_8(L^{naph})_{12}][BF_4]_{16}$, no diffusion of aromatic components is taking place, and the emission must be coming from a preformed arrangement in which the emissive excited state of the naphthyl chromophore is lowered in energy by interaction with the adjacent electron-deficient pyrazolyl-pyridine units in the π-stacks. Thus, the most likely assignment for this low-energy emission feature is that it arises from a naphthyl (donor) → pyridyl-pyrazole (acceptor) charge-transfer excited state in the preformed π-stacked ligand array, in contrast to the more intense 340 nm feature, which is pure naphthalene-based $\pi-\pi^*$ fluorescence.

The balance between the normal and exciplex-like fluorescence components varied with excitation wavelength, as shown in Figure 12 in which the spectra are normalized to the 340 nm emission band. This reflects the presence of the underlying charge-transfer absorption band which, although not apparent as a distinct transition in the absorption spectrum of $[Cd_8(L^{naph})_{12}][BF_4]_{16}$ because of its weakness compared to the fully allowed $\pi-\pi^*$ transitions, must be at lower energy than the naphthyl-based $\pi-\pi^*$ transition. An excitation spectrum, monitoring the luminescence intensity at 500 nm where only the exciplex component is contributing, revealed a maximum at ~300 nm (inset to Figure 12). We can say therefore that there is a naphthyl (donor) → pyridyl-pyrazole (acceptor) charge-transfer band centered at 300 nm hidden under the more intense $\pi-\pi^*$ transitions, and lower in energy than the lowest

(13) (a) Constable, E. C.; Martínez-Máñez, R.; Cargill Thompson, A. M. W.; Walker, J. V. *J. Chem. Soc., Dalton Trans.* **1994**, 1585. (b) Constable, E. C.; Daniels, M. A. M.; Drew, M. G. B.; Tocher, D. A.; Walker, J. V.; Wood, P. D. *J. Chem. Soc., Dalton Trans.* **1993**, 1947. (c) Amouri, H.; Mimassi, L.; Rager, M. N.; Mann, B. E.; Guyard-Duhayon, C.; Raehm, L. *Angew. Chem., Int. Ed.* **2005**, *44*, 4543.

(14) Harano, K.; Hiraoka, S.; Shionoya, M. *J. Am. Chem. Soc.* **2007**, *129*, 5300.

(15) Lakowicz, J. R. *Principles of Fluorescence Spectroscopy*, 3rd ed.; Springer: New York, 2006.

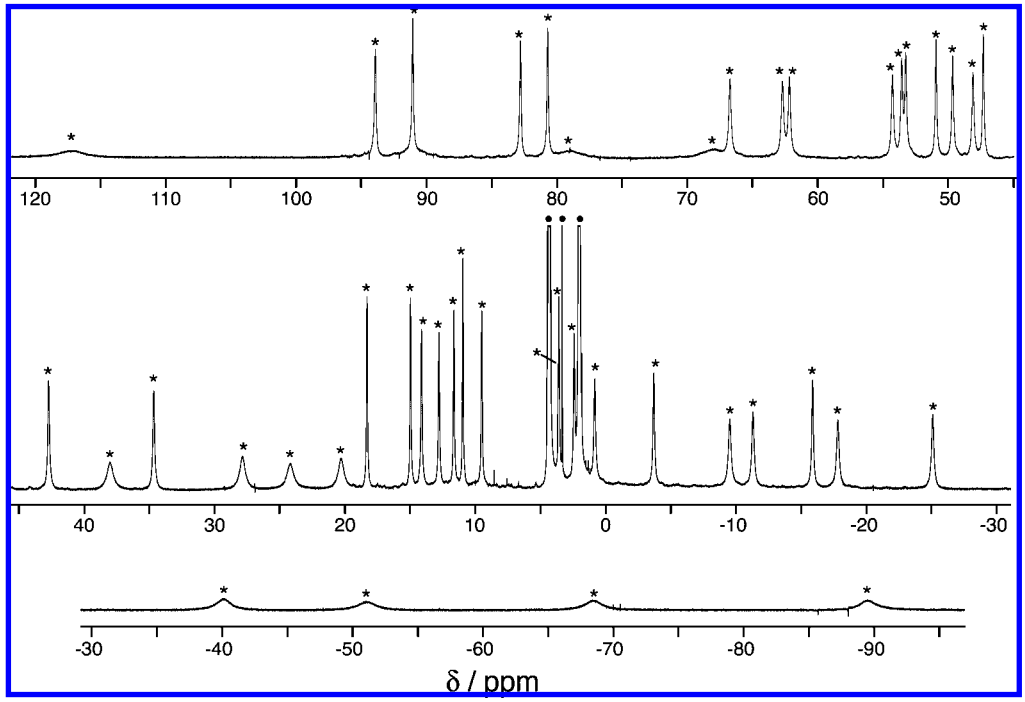

Figure 10. 400 MHz ^{1}H NMR spectrum of $[Co_8(L^{naph})_{12}][BF_4]_{16}$ in CD_3NO_2 showing 44 inequivalent signals in the range −90 to +120 ppm. The 44 peaks from the complex are labelled with an asterisk. The three peaks labelled with a dot between 0 and 5 ppm are from traces of protonated solvents.

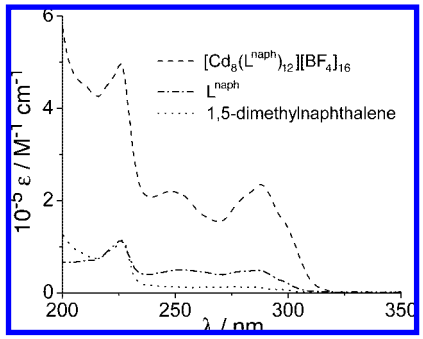

Figure 11. UV/vis absorption spectra of $[Cd_8(L^{naph})_{12}][BF_4]_{16}$ and free L^{naph} in MeCN.

naphthyl-centered $\pi-\pi^*$ transition at ∼275 nm, which is responsible for the exciplex-like component of the luminescence spectrum.[10]

3. Conclusions

Both types of ligand, L^{anth} and L^{naph}, react with first row transition metal dications to afford molecular cages of M_8L_{12} stoichiometry having an approximately cubic array of metal ions with a bridging ligand spanning each of the twelve edges. Despite the gross similarity between the two types of cage, there are important differences in structure and solution stability, as follows:

3.1. $[M_8(L^{anth})_{12}](BF_4)_{16}$ (M = Cu, Zn) have two cyclic helical $\{M_4(L^{anth})_4\}$ units of opposite chirality connected by four additional L^{anth} ligands as "pillars"; all metal centers have a *meridional* tris-chelate geometry. In contrast $[M_8(L^{naph})_{12}][BF_4]_{16}$ (M = Co, Ni, Cd) have noncrystallographic S_6 symmetry in which a diagonally opposed pair of metal centers (which lie on the S_6 axis) have a *facial* tris-chelate coordination geometry, whereas the other six metal centers are *meridional*.

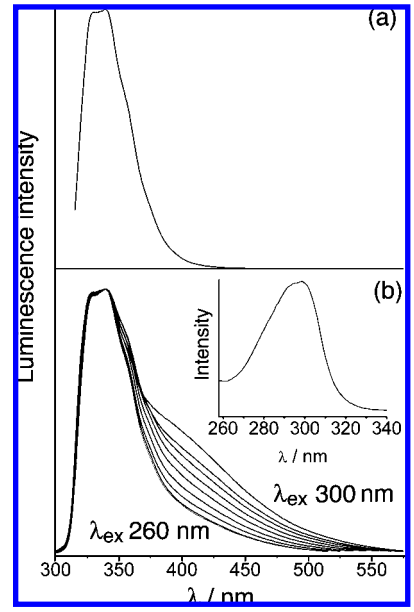

Figure 12. Normalized fluorescence spectra of (a) free L^{naph}; (b) $[Cd_8(L^{naph})_{12}][BF_4]_{16}$ using different excitation wavelengths from 260 to 300 nm at 5 nm intervals (inset is the excitation spectrum obtained when monitoring the exciplex emission at 500 nm). Solvent was MeCN in all cases.

3.2. $[M_8(L^{anth})_{12}](BF_4)_{16}$ are unusual among this general class of cage complexes for having no interligand π-stacking between electron-rich and electron-poor components. In contrast, in $[M_8(L^{naph})_{12}][BF_4]_{16}$ there is extensive stacking involving alternating electron-rich (naphthyl units) and electron-poor (pyridyl-pyrazole units coordinated to M^{2+} ions) components which assemble into six five-component stacks. This interaction is reflected in long-wavelength exciplex-like features in the fluorescence spectra of the Cd(II) cage, arising from naphthyl

(donor) → pyridyl-pyrazole (acceptor) charge-transfer transitions, which are not apparent for the free ligand.

3.3. Whereas $[M_8(L^{anth})_{12}](BF_4)_{16}$ do not appear to retain their structural integrity in polar solvents, giving messy NMR spectra and only fragment ions in ES mass spectra, $[M_8(L^{naph})_{12}][BF_4]_{16}$ do retain their structural integrity in solution. There are clear sequences of peaks in ES mass spectra corresponding to intact cages associated with different numbers of anions, and (for M = Co, Cd) NMR spectra showing 44 independent proton environments, as required by the S_6 symmetry revealed in the crystal structures. This is further supported by the ^{113}Cd NMR spectrum of the Cd(II) cage which reveals two Cd environments in a 1:3 ratio, due to the mixture of *facial* and *meridional* tris-chelate environments in that proportion. We suggest that the robustness of the cage structure of $[M_8(L^{anth})_{12}](BF_4)_{16}$ in competitive polar solvents is a direct consequence of the additional thermodynamic stability associated with the interligand aromatic stacking interactions.

4. Experimental Section

4.1. General Details. The compounds 1,5-bis(bromomethyl)-naphthalene,[16] 9,10-bis(bromomethyl)anthracene,[17] and 3-(2-pyridyl)pyrazole[18] were prepared according to previously published methods. ^{1}H NMR spectra and 2-D COSY spectra were recorded at 500 MHz on a Bruker DRX-500 spectrometer; the ^{113}Cd NMR spectrum was recorded on a Bruker Avance-2 400 spectrometer. Electrospray mass spectra of complexes were measured on a Bruker MicroTOF mass spectrometer in positive ion mode. Samples were prepared at a concentration of ~2 mg/cm^3 in $MeNO_2$ or MeCN and analyzed by direct infusion using a Cole-Parmer syringe pump at a flow rate of 3 μL/min. Spectra were acquired over an *m/z* range of 50−4000; several scans were averaged to provide the final spectrum. UV/vis absorption spectra were measured on a Cary 50 spectrophotometer, and luminescence and excitation spectra, on a Jobin-Yvon Fluoromax 4 fluorimeter.

4.2. Synthesis of L^{anth}. To a solution of 9,10-bis(bromomethyl)-anthracene (0.50 g, 1.37 mmol) and 3-(2-pyridyl)pyrazole (0.40 g, 2.70 mmol) in THF (60 cm^3) was added aqueous NaOH (5.5 M; 5 cm^3). The resulting mixture was heated to reflux for 20 h and then allowed to cool to room temperature. On cooling, a bright-yellow solid precipitated that was collected by filtration and washed with cold THF to yield analytically pure L^{anth} (0.61 g, 89%). Anal. Calcd for $C_{32}H_{24}N_6$: C 78.0; H, 4.9; N, 17.1% Found: C, 77.7; H, 5.1; N, 16.4%. ESMS: *m/z* 493 $(M + H)^+$, 515 $(M + Na)^+$, 531 $(M + K)^+$. ^{1}H NMR (400 MHz, $CDCl_3$): δ 8.68 (2H, ddd, *J* 4.8, 1.8, 0.8; pyridyl H^6), 8.47 (4H, dd, *J* 7.2, 3.2; anthryl H), 8.01 (2H, d, *J* 8.0; pyridyl H^3), 7.78 (2H, td, *J* 7.6, 1.6; pyridyl H^4), 7.63 (4H, dd, *J* 7.0, 3.2; anthryl H), 7.24 (2H, ddd, *J* 7.6, 4.8, 0.8, pyridyl H^5), 7.00 (2H, d, *J* 2.4; pyrazolyl H^5) 6.75 (2H, d, *J* 2.4 Hz; pyrazolyl H^4), 6.46 (4H, s; CH_2).

4.3. Synthesis of L^{naph}. L^{naph} was prepared using 1,5-bis(bromomethyl)naphthalene and 2.1 equiv of 3-(2-pyridyl)pyrazole exactly according to the method described above for L^{anth}. Pure L^{naph} precipitated from the reaction mixture on allowing it to cool to room temperature and was collected by filtration, washed with cold THF, and dried to yield an analytically pure product (0.63 g, 90%). Anal. Calcd for $C_{28}H_{22}N_6$: C 76.0; H, 5.0; N, 19.0% Found: C, 75.8; H, 5.0; N, 18.7%. ESMS: *m/z* 443 $(M + H)^+$, 465 $(M + Na)^+$. ^{1}H NMR (400 MHz, $CDCl_3$): δ 8.67 (2H, ddd, *J* 4.4, 2.4, 0.6; pyridyl H^2), 8.08 (2H, d, *J* 8.8; naphthyl $H^{2/4}$), 8.0 (2H, dt, *J* 8.0, 0.8; pyridyl H^3), 7.75 (2H, td, *J* 7.7, 2.0; pyridyl H^4), 7.51 (2H, dd, *J* 7.2, 1.2; naphthyl H^3), 7.36 (2H, d, *J* 7.2; naphthyl $H^{2/4}$), 7.28 (2H, d, *J* 1.9; pyrazolyl H^5), 7.19 (2H, ddd, *J* 7.5, 4.8, 0.8; pyridyl H^5), 6.88 (2H, d, *J* 2.0 Hz; pyrazolyl H^4), 5.90 (4H, s; CH_2).

4.4. Complex Syntheses. All complexes were prepared by either conventional or solvothermal methods; the preparation of $[Cu_8(L^{anth})_{12}][BF_4]_{16}$ is described as an example.

Solutions of $Cu(BF_4)_2 \cdot xH_2O$ (0.022 g, 0.07 mmol) in MeOH (7.5 cm^3) and L^{anth} (0.050 g, 0.1 mmol) in chloroform (7.5 cm^3) were combined, and the resulting solution was vigorously stirred for 24 h at room temperature. The solvent was subsequently removed under reduced pressure, and the crude solid was washed with methanol and then chloroform to remove any unreacted starting materials. Diethyl ether was allowed to slowly diffuse into a solution of the dried green powder in nitromethane. X-ray quality green prismatic crystals of $[Cu_8(L^{anth})_{12}][BF_4]_{16} \cdot 10MeNO_2$ grew on standing within one week.

Alternatively, a solvothermal method could be used which, for the complexes with L^{naph}, tended to afford larger and better quality crystals for X-ray diffraction studies. A representative method is as follows. A Teflon-lined autoclave was charged with $Ni(BF_4)_2 \cdot xH_2O$ (0.022 g, 0.07 mmol), L^{naph} (0.049 g, 0.11 mmol, and methanol (9 cm^3). Heating to 150 °C for 12 h followed by slow cooling to room temperature yielded large purple X-ray quality prismatic crystals of $[Ni_8(L^{naph})_{12}][BF_4]_{16} \cdot 5MeOH$ directly from the cooled reaction mixture in 90% yield.

Characterization data are as follows. The vacuum-dried samples of cage complexes were hygroscopic, presumably due to uptake of water into the large cavities and voids previously occupied by solvent molecules (cf. the crystal structures). Accordingly the elemental analyses are consistent with the presence of several molecules of uncoordinated water in every case.

Data for $[Cu_8(L^{anth})_{12}][BF_4]_{16}$. Yield: 52%. Found: C, 56.9; H, 3.7; N, 12.5. Required for $C_{384}H_{288}B_{16}Cu_8F_{64}N_{72} \cdot (H_2O)_{15}$: C, 57.1; H, 4.0; N, 12.5.

Data for $[Zn_8(L^{anth})_{12}][BF_4]_{16}$. Yield: 56%. Found: C, 55.5; H, 3.8; N, 12.1. Required for $C_{384}H_{288}B_{16}F_{64}N_{72}Zn_8 \cdot (H_2O)_{25}$: C, 55.7; H, 4.1; N, 12.2.

Data for $[Co_8(L^{naph})_{12}][BF_4]_{16}$. Yield: 81%. ESMS: see Figure 7. Found: C, 53.3; H, 3.9; N, 13.3. Required for $C_{336}H_{264}B_{16}F_{64}N_{72}Co_8 \cdot (H_2O)_{20}$: C, 53.6; H, 4.1; N, 13.4.

Data for $[Ni_8(L^{naph})_{12}][BF_4]_{16}$. Yield: 78%. ESMS: *m/z* 3498.8, $\{[Ni_8(L^{naph})_{12}][BF_4]_{14}\}^{2+}$; 2303.3, $\{[Ni_8(L^{naph})_{12}][BF_4]_{13}\}^{3+}$; 1705.2, $\{[Ni_8(L^{naph})_{12}][BF_4]_{12}\}^{4+}$; 1346.8, $\{[Ni_8(L^{naph})_{12}][BF_4]_{11}\}^{5+}$; 1108.1, $\{[Ni_8(L^{naph})_{12}][BF_4]_{10}\}^{6+}$. Found: C, 52.2; H, 3.8; N, 12.8%. Required for $C_{336}H_{264}B_{16}F_{64}N_{72}Ni_8 \cdot (H_2O)_{25}$: C, 53.0; H, 4.2; N, 13.2.

Data for $[Cd_8(L^{naph})_{12}][BF_4]_{16}$. Yield: 88%. ESMS: *m/z* 3712.8, $\{[Cd_8(L^{nap})_{12}][BF_4]_{14}\}^{2+}$; 2446.2, $\{[Cd_8(L^{nap})_{12}][BF_4]_{13}\}^{3+}$; 1812.4, $\{[Cd_8(L^{nap})_{12}][BF_4]_{12}\}^{4+}$; 1433.2, $\{[Cd_8(L^{nap})_{12}][BF_4]_{11}\}^{5+}$. Found: C, 49.5; H, 3.5; N, 12.1. Required for $C_{336}H_{264}B_{16}F_{64}N_{72}Cd_8 \cdot (H_2O)_{26}$: C, 50.0; H, 3.9; N, 12.5.

4.5. X-ray crystallography. Crystals were removed from the mother liquor, coated with oil, and transferred to a stream of cold N_2 on the diffractometer as quickly as possible to prevent decomposition due to solvent loss. All structural determinations except $[Cu_8(L^{anth})_{12}][BF_4]_{16} \cdot 10MeNO_2$ were carried out at the University of Sheffield on a Bruker SMART-APEX2 diffractometer using graphite-monochromated Mo Kα radiation ($\lambda = 0.71073$ Å) from a sealed-tube source. The data for $[Cu_8(L^{anth})_{12}][BF_4]_{16} \cdot 10MeNO_2$ were collected at the Daresbury Synchrotron Radiation Source (station 9.8) on a Bruker SMART-APEX2 diffractometer and Si(111)-monochromated synchrotron radiation with a wavelength ($\lambda = 0.6926$ Å) close to the Zr absorption edge.

Crystals of the metal complexes scattered relatively weakly due to the extensive disorder of anions and solvent molecules. After integration of the raw data, and before merging, an empirical

(16) Fleming, R. H.; Quina, F. H.; Hammond, G. S.; George, S. *J. Am. Chem. Soc.* **1974**, *96*, 7738.
(17) Gunnlaugsson, T.; Davisab, A. P.; O'Briena, J. E.; Glynna, M. *Org. Biomol. Chem.* **2005**, *3*, 48.
(18) (a) Amoroso, A. J.; Cargill Thompson, A. M. W.; Jeffery, J. C.; Jones, P. L.; McCleverty, J. A.; Ward, M. D. *J. Chem. Soc., Chem. Commun.* **1994**, 2751. (b) Brunner, H.; Scheck, T. *Chem. Ber.* **1992**, *125*, 701. (c) Lin, Y.; Lang, S. A. *J. Heterocycl. Chem.* **1977**, *14*, 345.

Table 1. Crystal parameters, data collection[a] and refinement details for the structures in this paper

compound	L^{anth}	L^{naph}	$[Zn_8(L^{anth})_{12}][BF_4]_{16}\cdot 15MeNO_2\cdot Et_2O$
formula	$C_{32}H_{24}N_6$	$C_{28}H_{22}N_6$	$C_{403}H_{343}B_{16}F_{64}N_{87}O_{31}Zn_8$
molecular weight	492.57	442.52	8812.56
T, K	100(2)	296(2)	100(2)
crystal system, space group	orthorhombic, *Pbca*	triclinic, $P\bar{1}$	triclinic, $P\bar{1}$
a, Å	10.7709(15)	9.8274(12)	26.5388(14)
b, Å	11.1673(18)	10.3168(12)	26.5941(13)
c, Å	19.954(4)	17.424(2)	30.384(2)
α, deg	90	82.862(9)	99.664(3)
β, deg	90	77.587(8)	113.727(3)
γ, deg	90	75.293(8)	110.117(2)
V, Å^3	2400.1(7)	1664.2(4)	17224.3(17)
Z	4	3	1
ρ, g cm^{-3}	1.363	1.325	0.85
crystal size, mm^3	0.30 × 0.30 × 0.05	0.25 × 0.25 × 0.10	0.80 × 0.40 × 0.40
μ, mm^{-1}	0.083	0.082	0.336
data, restraints, parameters	1712, 0, 172	8369, 0, 460	48618, 854, 2368
final R1, wR2[b]	0.0324, 0.0779	0.0513, 0.1643	0.1056, 0.3114

compound	$[Cu_8(L^{anth})_{12}][BF_4]_{16}\cdot 10MeNO_2$	$[Co_8(L^{naph})_{12}][BF_4]_{16}\cdot 6MeOH$	$[Ni_8(L^{naph})_{12}][BF_4]_{16}\cdot 5MeOH$
formula	$C_{394}H_{318}B_{16}Cu_8F_{64}N_{82}O_{20}$	$C_{342}H_{288}B_{16}Co_8F_{64}N_{72}O_6$	$C_{341}H_{284}B_{16}F_{64}N_{72}Ni_8O_5$
molecular weight	8418.58	7362.84	7329.04
T, K	120(2)	100(2)	100(2)
crystal system, space group	monoclinic, *C*2/*m*	monoclinic, *C*2/*c*	monoclinic, *C*2/*c*
a, Å	44.45(2)	32.9366(13)	33.0351(15)
b, Å	30.288(15)	29.9278(12)	29.5646(14)
c, Å	31.745(16)	39.8346(15)	39.8684(18)
α, deg	90	90	90
β, deg	124.280(6)	96.502(2)	97.011(2)
γ, deg	90	90	90
V, Å^3	35314(30)	39013(3)	38647(3)
Z	2	4	4
ρ, g cm^{-3}	0.792	1.254	1.26
crystal size, mm^3	0.20 × 0.10 × 0.10	0.50 × 0.50 × 0.50	0.60 × 0.50 × 0.25
μ, mm^{-1}	0.251	0.422	0.472
data, restraints, parameters	21927, 848, 1084	25506, 146, 1985	44383, 215, 2017
final R1, wR2[b]	0.1097, 0.3137	0.0733, 0.2146	0.0853, 0.2716

[a] All structures were collected using Mo Kα radiation (λ = 0.71073 Å), apart from $[Cu_8(L^{anth})_{12}][BF_4]_{16}\cdot 10MeNO_2$ for which synchrotron radiation was used (λ = 0.6926 Å), see Experimental Section. [b] The value of R1 is based on "observed" data with $I > 2\sigma(I)$; the value of wR2 is based on all data.

absorption correction was applied (SADABS)[19] based on comparison of multiple symmetry-equivalent measurements. The structures were solved by direct methods and refined by full-matrix least-squares on weighted F^2 values for all reflections using the SHELX suite of programs.[20] Pertinent crystallographic data are collected in Table 1. Lists of bond distances and angles in the metal ions' coordination spheres are in Supporting Information, as are pictures of the crystal structures of the two ligands L^{naph} and L^{anth}.

In $[Zn_8(L^{anth})_{12}][BF_4]_{16}\cdot 15MeNO_2\cdot Et_2O$ the asymmetric unit contains one-half of the complex cage. One of the four independent anthracenyl groups is disordered over two closely spaced sites with the site occupancies being ~0.69 and 0.31; another is similarly disordered with site occupancies of 0.37 and 0.63 over the two orientations, such that in total four of the twelve anthracenyl groups exhibit disorder. These anthracenyl groups required restraints to keep their geometries reasonabl, and the atoms concerned were refined with isotropic displacement parameters. Only 4.5 (four with 100% occupancy, one with 50% occupancy) of the expected eight $[BF_4]^-$ anions could be located in the asymmetric unit. Uncoordinated solvent molecules were assigned site occupancies of 50% or 100, as required to give reasonable displacement parameters, and were refined isotropically. In $[Cu_8(L^{anth})_{12}][BF_4]_{16}\cdot 10MeNO_2$ there was no anthracene disorder, but only one of the expected four independent $[BF_4]^-$ anions could be located in the asymmetric unit. Uncoordinated solvent molecules were refined isotropically. Additional extensive areas of residual electron density which could not sensibly be modeled as solvent or anions were removed *via* application of the "Squeeze" function in PLATON.[21] More details are given in the CIF files.

In each, $[Co_8(L^{naph})_{12}][BF_4]_{16}\cdot 6MeOH$ and $[Ni_8(L^{naph})_{12}][BF_4]_{16}\cdot 5MeOH$, half of the molecule constitutes the asymmetric unit; five and six, respectively, of the expected eight anions could be located. Again, anions and uncoordinated solvent molecules were refined isotropically and subjected to heavy restraints to keep their geometries reasonable.

Structural determinations of L^{naph} and L^{anth} were straightforward and presented no problems.

Acknowledgment. We thank the EPSRC (U.K.) for a postdoctoral research fellowship (to I.T.), and for funding of the U.K. National Crystallography Service. We also thank STFC (U.K.) for access to synchrotron facilities.

Supporting Information Available: Lists of bond distances and angles in the metal ions' coordination spheres, graphics of the crystal structures of the two ligands L^{naph} and L^{anth}, and X-ray crystallographic files in CIF format. This material is available free of charge via the Internet at http://pubs.acs.org.

JA805605Y

(19) Sheldrick, G. M. *SADABS: A program for absorption correction with the Siemens SMART system*; University of Göttingen: Germany, 1996.
(20) Sheldrick, G. M. *Acta Crystallogr., Sect. A* **2008**, *64*, 112.
(21) Spek, A. L. *J. Appl. Crystallogr.* **2003**, *36*, 7.